Electronic Supplementary Information

Electronic Redistribution Induced by Interaction between Ruthenium Nanoparticles and Ni-N(O)-C Sites Boosts Alkaline Water Electrolysis

Jiacheng Wang, [a, b] Wangtao He, [b] Yuyang Zong, [c] Yanfeng Tang, [d] Jin Wang, [d] and Ruguang Ma [c,*]

a. Zhejiang Key Laboratory for Island Green Energy and New Materials, Institute of Electrochemistry, School of Materials Science and Engineering, Taizhou University, Taizhou 318000, Zhejiang, China.

b. State Key Laboratory of High-Performance Ceramics and Superfine Microstructure, Shanghai Institute of Ceramics, Chinese Academy of Sciences, Shanghai 200050, China

c. School of Materials Science and Engineering, Suzhou University of Science and Technology, 99 Xuefu Road, Suzhou 215011, China. E-mail: ruguangma@usts.edu.cn

d. College of Chemistry and Chemical Engineering, Nantong University, Nantong 226019, China

Experimental section

Chemicals and materials

Dicyandiamide ($C_2H_4N_4$, 99%) and Nafion solution (5 wt.%) were purchased from Aldrich. $RuCl_3 \cdot xH_2O$ (35-42%) and $NiCl_2 \cdot 6H_2O$ (≥98.0%) were purchased from Sinopharm Chemical Reagent Co., Ltd. Multiwall carbon nanotubes (MWCNTs) were purchased from XFNANO Inc. All reagents were used as received without further purification.

Materials synthesis

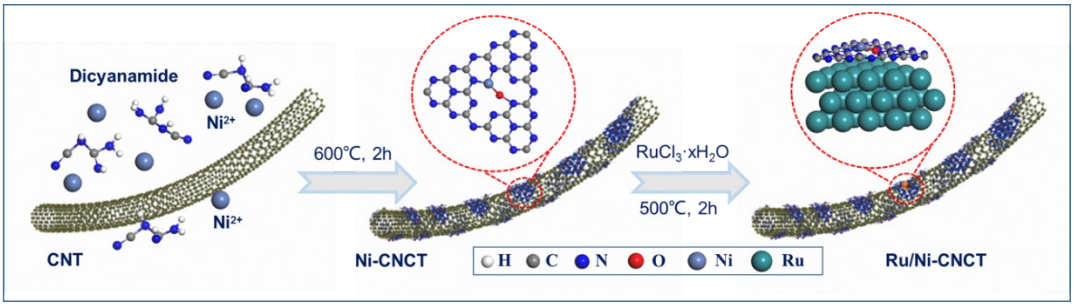

Fig. S1 Illustration of synthetic process of Ru/Ni-CNCT.

The synthesis process is illustrated in Fig. S1. Firstly, 0.2 g dicyandiamide was dissolved into deionized water (15 mL) at 100 °C under magnetic stirring until a transparent solution was formed. Then, 0.1 g MWCNTs were dispersed into the above solution. Afterwards, a certain amount of $NiCl_2 \cdot 6H_2O$ (3.025 mg, 12.10 mg corresponding to 0.5 wt.% and 1 wt.%, respectively) was added and ultrasonically dissolved into the solution. Subsequently, the as-formed solution was dried at 100 °C until a black powder was obtained. Afterward, this powder was placed in an alumina boat in a quartz tube furnace and heated at 600 °C for 2h with a ramp of 5 °C min^{-1} in Ar gas atmosphere to produce the final powder (denoted as Ni-CNCT).

To obtain Ru/Ni-CNCT, 0.1g Ni-CNCT was ultrasonically dispersed into deionized water (10 mL), followed by the addition and dissolution of 10.3 mg (5 wt.%) $RuCl_3 \cdot xH_2O$. After drying at 80 °C for 12 h, the as-obtained powder was transferred in an alumina boat in a quartz tube furnace and heated at 500 °C for 2h with a ramp of 5 °C min^{-1} in Ar gas atmosphere. After cooling to room temperature, the final powder was collected and named as Ru/Ni-CNCT. By changing the amount of $RuCl_3 \cdot xH_2O$,

the sample with different Ru loading was obtained. Similarly, Ru/Fe-CNCT and Ru/Co-CNCT were synthesized by replacing the $NiCl_2 \cdot 6H_2O$ with adequate amount of $FeCl_3$ or $Co(NO_3)_2 \cdot 6H_2O$.

Materials characterization

The morphology of the catalysts was observed by scanning electron microscopy (SEM) using on an FEI field emission Magellan 400 SEM equipped with an Oxford Instruments EDS system. Transmission electron microscopy (TEM), high-resolution TEM (HRTEM), high angle annular dark-field scanning TEM (HADDF-STEM), and energy-dispersive X-ray spectroscopy (EDS) mapping were taken on JEOL JEM 2100F transmission electron microscope operating at an accelerating voltage of 200 kV with an Oxford Instruments energy-dispersive X-ray spectrometer.

X-ray powder diffraction (XRD) measurements were carried out on a Rigaku D/MAX-2250V diffractometer with Cu K_α radiation. X-ray photoelectron spectroscopy (XPS) was recorded with an ESCALAB 250 X-ray photoelectron spectrometer with Al Kα ($h\upsilon$ = 1486.6 eV) radiation. All spectra were calibrated using 284.5 eV as the line position of adventitious carbon. For each sample, the XPS measurements were performed three times. Raman spectra were recorded on a DXR Raman Microscope (Thermal Scientific Co., USA) with 532 nm excitation length. X-ray absorption fine structure (XAFS) spectra at the Ni K-edge were obtained at the Canadian Light Source, beamlines SXRMB and BioXAS, respectively. The samples were pressed into pellets and measured in the transmission mode. For surface sensitive probe, XAFS data was collected as total electron yield. The data were processed with the ATHENA program for background subtraction, normalization and energy calibration. The extended XAFS (EXAFS) was processed using the IFEFFIT package. The EXAFS fitting was performed in R-space between 0.1 Å and 3.4 Å (the Fourier transform from k-space was performed over a range of 0.5 to 11.5 $Å^{-1}$).

Electrochemical measurements

Electrochemical measurements were performed in a three-electrode electrochemical

cell using a CHI 760E electrochemical workstation. A saturated calomel electrode (SCE) and a graphite rod were used as the reference elect rode and counter electrode, respectively. The working electrode was prepared as follows. The active material (5 mg) was dispersed in the mixture of water (0.25 mL) and ethanol (0.25 mL) containing 5% Nafion solution (25 μL) under ultrasonic irradiation for ca. 1 h until a homogeneous ink was formed. Then, 5 μL ink containing 50 μg catalyst was transferred onto a glassy carbon electrode (GCE) with 5 mm diameter, yielding a catalyst level of 0.25 mg cm^{-2}. The electrode with the catalyst was dried at 50 °C which was used as the working electrode for further electrochemical measurements. All the potentials vs. SCE were converted to versus reversible hydrogen electrode (RHE) according to the following equation:

E (vs. RHE) = E (vs. SCE) +1.06 V (1)

Before recording, the working electrode was scanned for 20 cycles in Ar gas saturated 1.0 M KOH solution until a stable cyclic voltammogram was recorded. Linear sweep voltammetry (LSV) polarization curves were recorded at a scan rate of 5 mV s^{-1}. All polarization profiles were corrected with 80% iR compensation. Electrochemical impedance spectroscopy (EIS) was conducted on charged catalysts at 0.5 V vs. SCE over a frequency range from 1 to 100 kHz. The electrochemically active surface area of samples was estimated from the slope of the C_{dl} value. Cyclic voltammetry (CV) was measured at a scan rate of 20 ~ 180 mV s^{-1} in the voltage window from -0.96 V to -0.75 V. The Tafel slopes were obtained from the treatment of the polarization curve based on the Tafel equation:

$\eta = a + b \log j$ (2)

where η is the overpotential, a is the intercept, b is the Tafel slope and j is the current density.

The H_2 and O_2 gas were collected by the water drainage method. A constant current density (10 mA cm^{-2}) was applied on the electrode and the volume of evolved gases was recorded synchronously. Faradic efficiency (FE) is calculated to be the ratio of the amount of experimentally determined hydrogen to that of the theoretically expected hydrogen as follows.[1]

$$FE = \frac{V_{exp.}}{V_{thero.}} = \frac{V_{exp.}}{\frac{n}{4} \times \frac{Q}{F} \times V_m} \quad (3)$$

where Q is the charge passed through the electrode, F is Faraday constant (96485 C mol^{-1}), the number 4 means 4 mole electrons per mole O_2, the number n=1 means 1 mole of O_2 or n=2 means 2 moles of H_2, V_m is molar volume of gas (24.5 L mol^{-1}, 298 K, 101 KPa).

DFT calculations

The density functional theory calculations were performed by Vienna ab initio simulation package (VASP) program with projector augmented wave (PAW) method and the kinetic energy cutoff was set to be 450 eV.[2] A mesh of 2 × 2 × 1 was used for the k-point sampling obtained from the Gamma center. Structure models of Ru (001) and Ru/Ni-CNCT are constructed on the basis of HRTEM image and the thickness of the vacuum layer is 20 Å. The atomic positions were fully optimized until the energy and forces are converged to 1×10^{-4} eV and 0.05 eV $Å^{-1}$, respectively. The calculations of binding energy of HER intermediates were conducted following method which was used by Nørskov[3]:

$\Delta G = \Delta E + \Delta E_{ZPE} - T\Delta S$ (4)

$\Delta E = E(H^*) - E(*) - E(H)$ (5)

where * is catalyst, H* is adsorbed H, $E(H) = 1/2\ E(H_2)$

E_{ZPE} is the zero-point energy, S is the entropy and T is the temperature (298K).

The binding energy is calculated as the energy difference between the adsorbed system and the sum of the slab and the free H_2O molecules:

$\Delta E_W = E_{total} - E_{slab} - E_{H2O}$ (6)

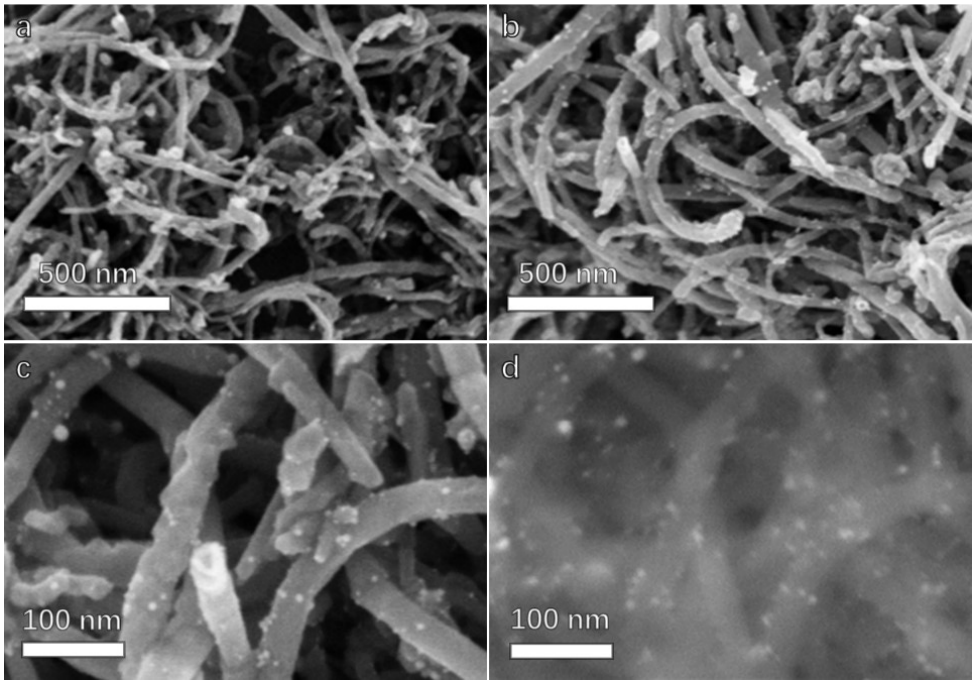

Fig. S2 SEM images of (a) Ni-CNCT and (b) Ru/Ni-CNCT, (c) enlarged SEM image and (d) back-scatting electron image of Ru/Ni-CNCT.

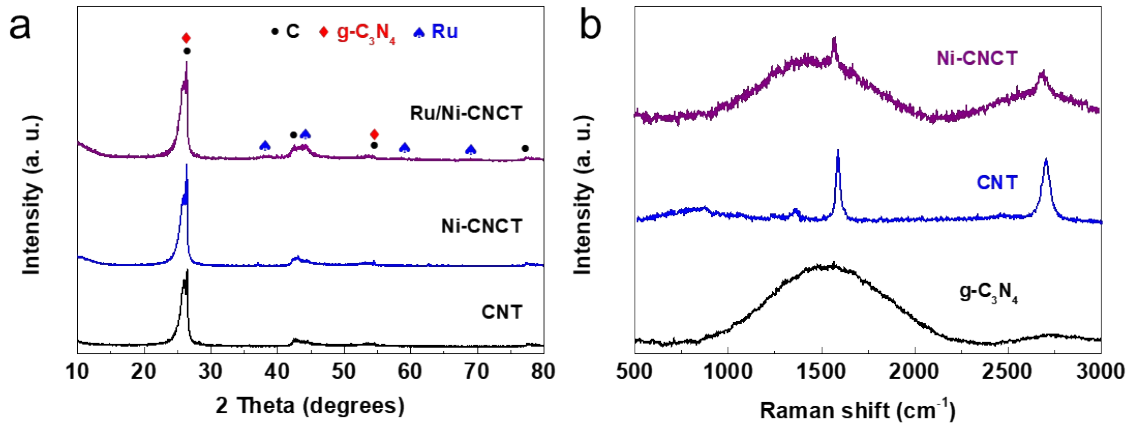

Fig. S3 (a) XRD patterns of Ru/Ni-CNCT, Ni-CNCT and carbon nanotubes; (b) Raman spectra of Ni-CNCT, CNT and g-C_3N_4.

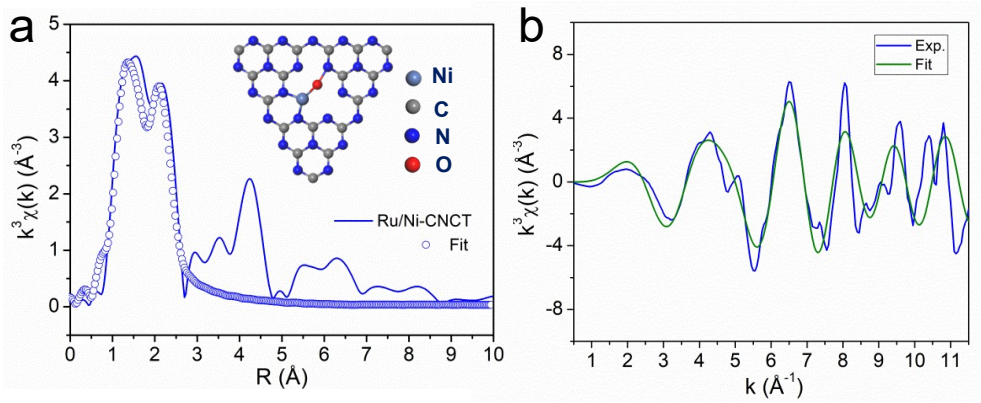

Fig. S4 EXAFS fitting results of Ni K-edge at (a) R space and (b) k-space.

Table S1. EXAFS fitting parameters at the Ni K-edge（S_0^2=0.82）

Sample	Path	C.N.	R (Å)	$\sigma^2\times10^3$ (Å^2)	ΔE (eV)	R factor
Ni foil	Ni-Ni	12*	2.48±0.01	6.1±0.1	7.2±0.3	0.001
Ru/Ni-CNCT	Ni-N/O	4.1±1.2	1.92±0.02	10.2±4.2	-4.7±3.0	0.019
	Ni-Ni	1.4±0.7	2.46±0.02	3.9±3.8	0.6±4.8	

[a]*N*: coordination numbers; [b]*R*: bond distance; [c]σ^2: Debye-Waller factors; [d] ΔE_0: the inner potential correction. *R* factor: goodness of fit. * the experimental EXAFS fit of metal foil by fixing CN as the known crystallographic value.

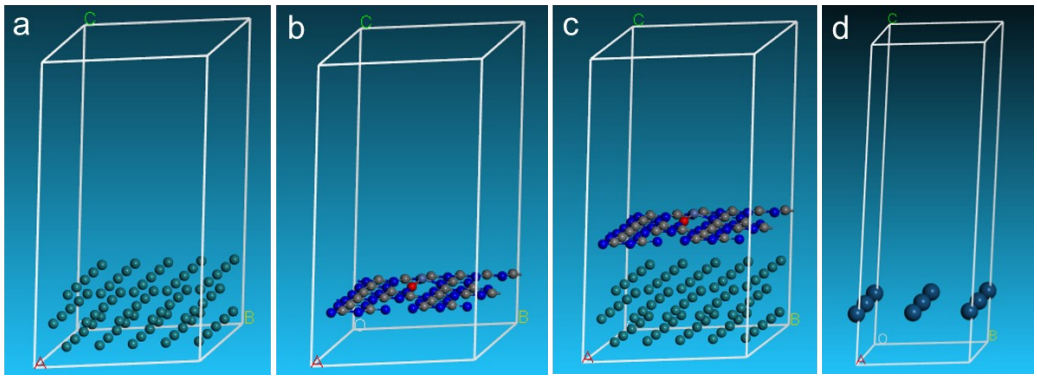

Fig. S5 Structure models of (a) Ru (001), (b) Ni-CNCT, (c) Ru/Ni-CNCT and (d) Pt(111).

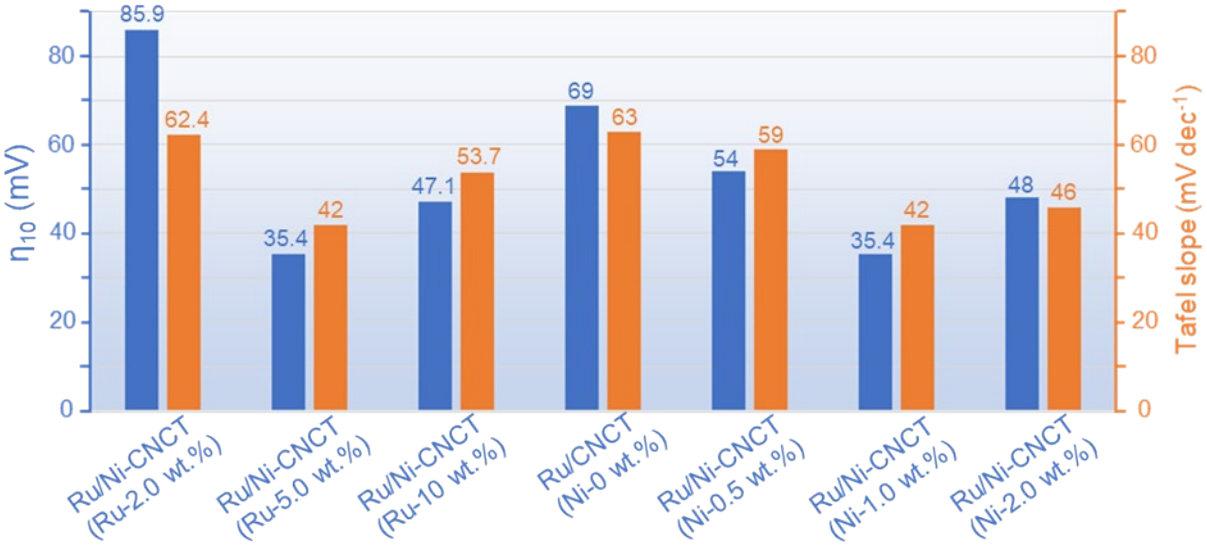

Fig. S6 Comparison of overpotentials at 10 mA cm^{-2} and Tafel slopes of the as-prepared samples with different Ru contents and Ni contents.

When the content of Ru is 5 wt.% and the content of Ni is 1.0 wt.%, respectively, the as-prepared Ru/Ni-CNCT exhibits the lowest Tafel plot and overpotential at 10 mA cm^{-2}, showing the best electrocatalytic performance among all the as-prepared samples (Fig. S6).

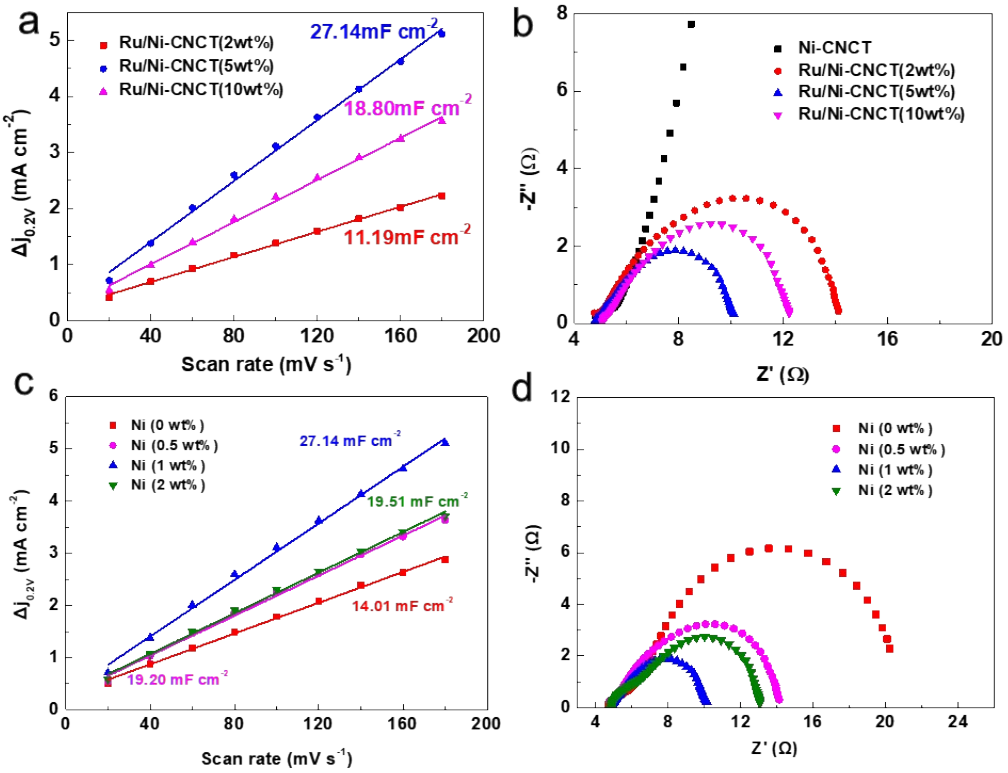

Fig. S7 Comparison of (a, b) double-layer capacitance and (b, d) EIS of the as-prepared samples with different Ru content and Ni content.

Moreover, the optimized Ru/Ni-CNCT (Ru-5wt% and Ni-1wt.%) shows the larger double-layer capacitance of (C_{dl}=27.14 mF cm^{-2}) than other samples (Fig. S7a & 7c), which implies that it has the largest electrochemically active surface area. Besides, the optimized Ru/Ni-CNCT shows the smallest semicircle in the electrochemical impedance spectra (Fig. S7b & 7d), indicating the lowest charge-transfer resistance among the as-prepared samples.

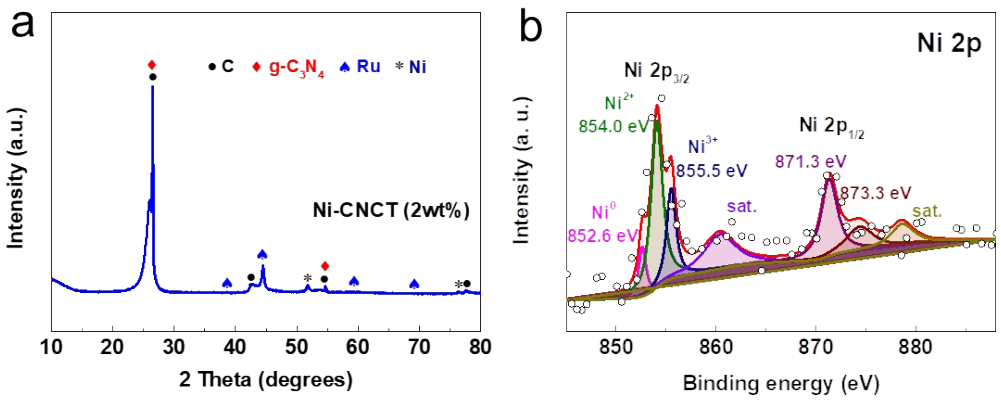

Fig. S8 (a) XRD pattern and (b) high-resolution XPS of Ni 2p of Ru/Ni-CNCT (Ni-2 wt.%).

XRD pattern reveals that with the increase of Ni content to 2 wt.%, there are obvious diffraction peaks assigned to metallic Ni (Fig. S8a). And there is also an obvious deconvoluted peak, which can be attributed to Ni^0 in the high-resolution XPS of Ni 2p (Fig. S8b).

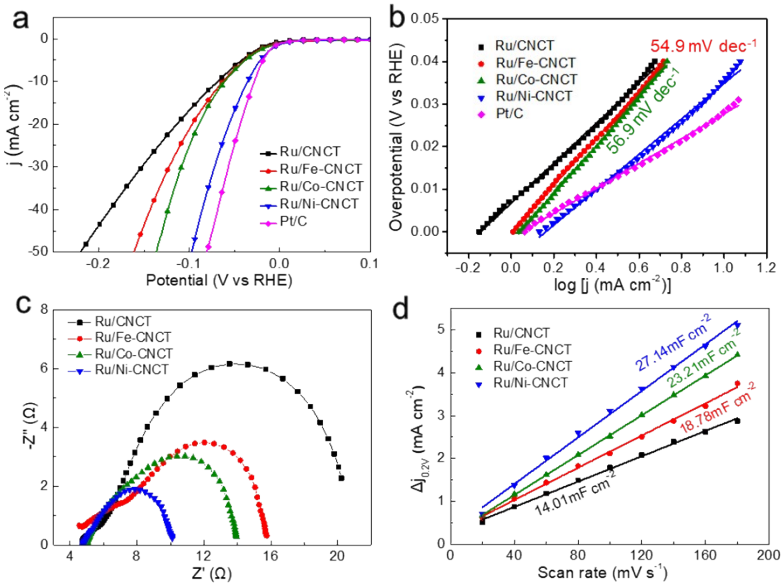

Fig. S9 Comparison of electrocatalytic performance of Ru/Fe-CNCT, Ru/Co-CNCT and Ru/Ni-CNCT. (a) LSV curves, (b) Tafel slopes, (c) EIS results and (d) double-layer capacitance of Ru/CNCT, Ru/Fe-CNCT, Ru/Co-CNCT and Ru/Ni-CNCT, respectively.

Other nanocomposites with Ru nanoparticles encapsulated by g-C_3N_4 layers with single-atom TM-N(O)-C sites on carbon nanotubes were also synthesized, such as Ru/Fe-CNCT and Ru/Co-CNCT (Fig. S9a). Among them, Ru/Ni-CNCT shows the best electrocatalytic activity, which is close to commercial Pt/C. The overpotential at 10 mA cm^{-2} of Ru/Fe-CNCT and Ru/Co-CNCT is 64.2 and 60.7 mV, respectively, much larger than that of Ru/Ni-CNCT (35.4 mV). The Tafel slope of Ru/Fe-CNCT and Ru/Co-CNCT is 54.9 and 56.9 mV dec^{-1}, respectively (Fig. S9b), larger than that of Ru/Ni-CNCT (42 mV dec^{-1}). Electrochemical impedance spectroscopy (EIS) results show that the charge-transfer resistance of Ru/Ni-CNCT is much smaller than those of Ru/CNCT, Ru/Fe-CNCT and Ru/Co-CNCT (Fig. S9c). And Ru/Ni-CNCT simultaneously possesses the largest C_{dl} (27.14 mF cm^{-2}), much larger than those of Ru/CNCT (14. 01 mF cm^{-2}), Ru/Fe-CNCT (18.78 mF cm^{-2}) and Ru/Co-CNCT (23.21 mF cm^{-2}), indicating the large ECSA and more active sites in Ru/Ni-CNCT (Fig. S9d).

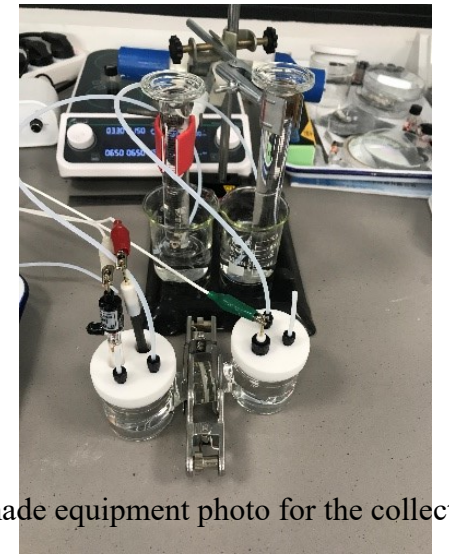

Fig. S10 Home-made equipment photo for the collection of H_2 and O_2.

References

[1] Z. Liu, D. Liu, L. Zhao, J. Tian, J. Yang, L. Feng, *Journal of Materials Chemistry A* **2021**, *9*, 7750-7758.

[2] G. Kresse, J. Furthmüller, *Computational Materials Science* **1996**, *6*, 15-50.

[3] J. K. Nørskov, T. Bligaard, A. Logadottir, J. R. Kitchin, J. G. Chen, S. Pandelov, U. Stimming, *J. Electrochem. Soc.* **2005**, *152*, J23-J26.